

Photovoltaic DC series arc fault detection method based on two-stage feature comprehensive decision

Bangzheng Han ^a, Guofeng Zou ^{a,*}, Wei Wang ^a, Jinjie Li ^b, Xiaofei Zhang ^a

^a School of Electrical and Electronic Engineering, Shandong University of Technology, 255049, Zibo, China

^b Pingyuan County Power Supply Company, State Grid Shandong Electric Power Company, 253100, Pingyuan, China



ARTICLE INFO

Keywords:

Photovoltaic power generation system

DC series arc fault detection

Signal windowing

Stage division

Transient feature

Steady-state feature

ABSTRACT

To address the issue of strong randomness and the difficulty in accurately describing fault features of photovoltaic power generation system series arc, a photovoltaic DC series arc fault detection method based on two-stage feature comprehensive decision is proposed. Firstly, to solve the difficulty in selecting fault detection window size due to the non-periodicity and high randomness of DC signals, a signal windowing strategy based on autocorrelation function is proposed. Based on the transient characteristics of arc initiation stage and the steady-state characteristics of arc burning stage, the whole arc stage is divided into transient stage and steady-state stage. Then, in the arc initiation stage, a transient feature description method based on adjacent windows difference (AWD) is designed on the basis of signal windowing, effectively capturing the waveform mutation caused by arc, achieving the fault occurrence window positioning and the effective expression of transient feature. In the arc burning stage, a steady-state feature description method based on energy difference (ED) is designed on the basis of signal windowing and fault occurrence window positioning, effectively capturing the energy difference caused by arc, achieving a significant expression of steady-state feature, and overcoming the misjudgment issues caused by transient feature. Finally, SVMs are used to classify the proposed features, and voting decision is combined to obtain the arc fault detection results. Experimental results show that the proposed method is feasible and effective in the feature extraction and detection of arc fault, providing a valuable approach for photovoltaic DC series arc fault detection.

1. Introduction

Against the backdrop of accelerating the achievement of the “dual carbon” goals, the installation and use of photovoltaic power generation systems have been increasing year by year [1]. With the rapid promotion of photovoltaic systems, the issue of arc faults in DC systems has become prominent [2]. Photovoltaic DC arc has no periodic zero-crossing, and the arc initiation process during a fault is brief, with an extremely short fault detection window period. Additionally, it is subject to interference from multiple factors in the system, making it difficult to effectively distinguish the arc fault current signal from the normal current signal that is affected by interference [3,4]. Therefore, to ensure the safe operation of photovoltaic systems and enhance the reliability of power supply [5,6], researching timely and reliable methods for detecting photovoltaic DC arc faults is of great significance.

Currently, series arc fault detection methods can be summarized into two categories: (1) Detection methods based on non-electrical quantities such as arc light, arc sound, and electromagnetic radiation [7–9]. (2) Detection methods based on electrical quantities such

as line current or voltage [10–21]. Among them, the former responds quickly and can achieve real-time monitoring of arc faults, but the installation environment of photovoltaic power generation systems is complex and changeable, this method has greater limitations. In detection methods based on electrical quantities, the location of arc occurrence is uncertain, and it is not easy to determine the line voltage monitoring point after a fault. Therefore, compared with the voltage detection method [10–12], arc fault detection based on current signals is more applicable and more favored by researchers.

The detection methods for DC series arc faults based on current signals are divided into three categories: (1) Arc fault detection methods based on time-domain features. These methods analyze and describe the time-domain waveform variations of the current signal and compare them with preset thresholds to identify faults, such as periodic mean change rate method [13] and time-domain waveform standard deviation method [14]. These methods are simple and have good real-time performance, but the waveform variations are affected by nonlinear loads, and it is difficult to set a unified threshold for fault identification. (2) Arc fault detection methods based on frequency

* Corresponding author.

E-mail address: gfzou@sdut.edu.cn (G. Zou).

domain features. These methods analyze and describe the frequency spectrum distribution of current signals, and identify fault signals by comparing the spectrum distribution or feature thresholds, such as the specific frequency spectrum amplitude method [15] and the frequency band amplitude method [16]. These methods are quite flexible, but the selection of fault frequency bands is susceptible to interference, and the threshold setting is often influenced by the sampling rate. (3) Arc fault detection methods based on time-frequency domain features. These methods capture fault components by performing time-frequency analysis on current signals, extract fault component features, and compare them with set thresholds to identify faults. Examples include the frequency band energy method [17] and the wavelet detail coefficient variance and modulus maxima method [18]. These methods offer good comprehensiveness, but the decomposition effect is difficult to ensure, and the rules for selecting fault components cannot be uniformly set.

Furthermore, researchers have effectively improved the accuracy and comprehensiveness of arc fault detection through comprehensive analysis. Huang et al. [19] extracted the frequency domain feature of wavelet energy and the time domain feature of current amplitude variance, then constructed a system feature plane for fault type differentiation, effectively overcame the interference of inverter switching frequency. Hu et al. [20] proposed using the rate of change of current mean in the time domain and the difference between the maximum and minimum values of the current cycle, as well as the energy and energy ratio of each frequency band in the frequency domain, and the modal component energy entropy in the time-frequency domain, to construct a feature space for arc fault detection, realized the comprehensive expression of arc fault features. Huang et al. [21] collected arc noise signals at the DC bus under various arc conditions, obtained corresponding arc fault features, and studied the arc signals from the time domain, frequency domain, and time-frequency domain to achieve comparative analysis of arc faults. Finally, it verified that the time-frequency domain-based detection method is more suitable for comprehensive analysis of arc faults.

Based on the above analysis, there has been considerable research on the detection methods for DC series arc faults, but most methods extract features from the overall current signal. On the one hand, this may introduce a large number of interfering features due to data redundancy, on the other hand, it may weaken the expression of key fault features, leading to the loss of effective features. Therefore, this paper comprehensively considers the process characteristics of DC series arc current, and divides the DC series arc into transient arc initiation stage and steady-state arc burning stage, then propose a photovoltaic DC series arc fault detection method based on two-stage feature comprehensive decision. The main contributions of this paper are as follows:

Firstly, considering the challenges of the non-periodicity and strong randomness of DC current, which makes it difficult to select the window size, a windowing strategy based on autocorrelation function is proposed. This strategy uses the periodicity and peak values of the normal current waveform's autocorrelation function to achieve window segmentation of DC arc fault currents.

Subsequently, features are extracted based on the results of stage division. In the extraction of transient feature, to address the issue of the difficulty in locating the fault occurrence window and the ineffective expression of transient feature, an adjacent windows difference (AWD) feature is defined based on the divided windows. By calculating the mean absolute value of the differences between adjacent windows, the fluctuation differences in the DC current can be accurately captured, achieving the positioning of the fault occurrence window and the effective description of transient fluctuation feature. In the extraction of steady-state feature, to address the issue that transient feature is prone to causing misjudgments, an energy difference (ED) feature is defined. Based on the signal windowing strategy, according to the located fault occurrence window, select the normal window with the smallest variance before the fault occurrence window, as well as

the fault window with the largest variance after the fault occurrence window, use the CEEMDAN algorithm to decompose the window signal and calculate the spectral kurtosis of each modal component, select the component with the largest spectral kurtosis as the optimal component, by calculating the energy difference between the optimal components of the window signal, the significant expression of the steady-state energy difference feature is achieved.

Finally, addressing the issue that threshold methods are susceptible to the complexity and diversity of signals as well as environmental factors, this paper adopts support vector machine(SVM) combined with voting decision method, overcoming the subjective selection of thresholds, achieving accurate detection of photovoltaic DC series arc faults. Experiments on actual measured datasets demonstrate that, the method proposed in this paper, overcoming the issue of strong randomness in current signals, effectively improving the accuracy of photovoltaic DC series arc fault detection.

2. Signal windowing strategy based on autocorrelation function

DC arc fault current signals are non-periodic and are influenced by the different lengths of the lines and the different nature of the downstream loads, exhibiting strong randomness and non-stationarity, making it difficult to select the size of the windowing. Therefore, this paper utilizes the time domain waveform of the normal current signal, then proposes a signal windowing method based on autocorrelation function to identify and analyze the recurring patterns in the signal, solving the segmentation problem of the arc fault current signal. The specific steps are as follows:

The normal DC signal is denoted as $x_1(n), n = 1, 2, \dots, N$, where N is the total number of sampling points. If the interval between two sampling points in the current signal sequence $x_1(n)$ is K , then the autocorrelation function of the current between the sampling points in the sequence is defined as follows:

$$\rho(K) = \frac{\sum_{i=1}^{N-K} ((x_1(i) - \mu) * (x_1(i+K) - \mu))}{N - K}, \quad 1 \leq K \leq \frac{N}{2} \quad (1)$$

$$\mu = \frac{\sum_{i=1}^N x_1(i)}{N} \quad (2)$$

Here, $\rho(K)$ is the autocorrelation value of the sequence $x_1(n)$ with a delay interval of K sample points, where K is the window size, $x_1(i)$ represents the i th sample point of the sequence $x_1(n)$, μ represents the mean value of the complete sequence $x_1(n)$.

After calculating the autocorrelation function, plot the autocorrelation function sequence diagram, and analyze the periodic patterns and peak value change rules of the waveform diagram. Look for periodic patterns in the signal, and at the same time, to ensure the strongest correlation within the window, select the peak position of the autocorrelation function as the windowing indicator. Therefore, the window size K is defined as follows:

$$K = \{T | \rho(T) = \rho_{peak}\} \quad (3)$$

Subsequently, calculate the variance σ^2 and mean μ of the complete sequence $x_1(n)$ to verify whether the selected window size K is reasonable.

$$\sigma^2 = \frac{\sum_{i=1}^N (x_1(i) - \mu)^2}{N} \quad (4)$$

Apply windowing processing to the complete sequence $x_1(n)$, where the window size is K and the number of windows is s . Calculate the mean and variance for each window, the formula is as follows:

$$\mu_j = \frac{\sum_{i=(j-1)K+1}^{jK} x_1^j(i)}{K}, \quad 1 \leq j \leq s \quad (5)$$

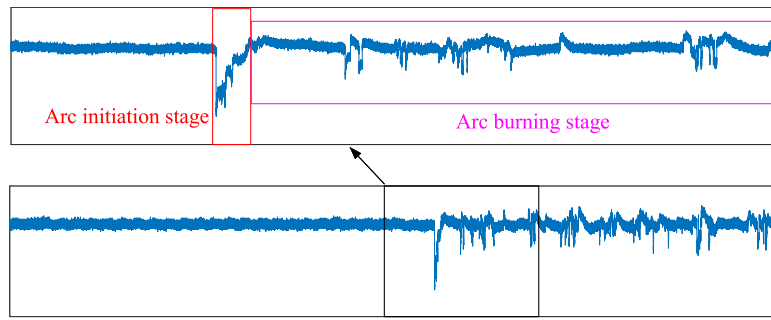


Fig. 1. Typical arc fault current waveform.

$$\sigma_j^2 = \frac{\sum_{i=(j-1)K+1}^{jK} (x_1^j(i) - \mu_j)^2}{K}, \quad 1 \leq j \leq s \quad (6)$$

After obtaining the means and variances of each window, compare the similarity of the means and variances between the normal current signal and each segmented window, as shown in Eq. (7):

$$err_j = |\mu - \mu_j| + |\sigma^2 - \sigma_j^2| \quad (7)$$

The smaller the value of err , the closer the mean and variance of the signal sequence within the segmented window are to those of the overall signal sequence, indicating that the statistical properties of the signal sequence within the segmented window are similar to those of the overall signal sequence. This suggests that there is no significant difference in the overall features of the signal within the window, which confirms that the selected window size is appropriate. On the contrary, it indicates that the selected window size is not suitable, necessitating the re-establishment of the windowing criteria and the selection of a new window size.

The windowing method for current signals based on autocorrelation function has achieved adaptive segmentation of photovoltaic DC arc fault current signals, avoiding the issue of an overly large window that cannot accurately capture the changing features of the arc fault current signal, and an overly small window that cannot accurately express the features of the arc fault current signal or may cause loss of features, providing a foundation for the subsequent description of arc fault features.

3. Arc fault stage feature extraction

The occurrence process of arc fault can be divided into the arc initiation stage and the arc burning stage. Fig. 1 shows a typical arc fault current waveform. The lower image is the complete DC arc signal with a duration of 1 s collected according to the UL1699B standard, and the upper image is a magnified view of a sub-window extracted from the full signal.

By observing the complete current signal, it is evident that the amplitude of the normal current and the arc current have the same amplitude, with the arc current showing continuous fluctuations due to plasma discharge. The arc initiation process is a very brief one, accompanied by severe fluctuations in the current waveform. During the arc initiation stage, the current amplitude changes abruptly, and the arc fault current signal exhibits distinct nonlinear and instantaneous transient characteristics. The arc burning process lasts for a longer duration, with the arc discharge phenomenon continuously present, leading to sustained fluctuations in the current waveform. During the arc burning stage, the current amplitude remains relatively stable, and the arc fault current signal exhibits steady-state characteristics. Therefore, to achieve effective detection of arc faults, the arc occurrence process is divided into transient and steady-state processes, feature extraction is performed for the arc occurrence process.

3.1. Transient feature extraction based on AWD

The arc initiation process in DC arc faults is brief, making it difficult to accurately locate the fault occurrence window and to precisely express transient feature. Therefore, this paper proposes a transient feature extraction method based on AWD on the basis of window division. By comparing the difference between adjacent windows, this method can more accurately capture the subtle changes in arc fault current signals, achieving the localization of the fault occurrence window and the effective description of transient fluctuation feature. The specific steps are as follows:

The DC arc fault current signal is denoted as $x_2(n)$, $n = 1, 2, \dots, N$, where N is the total number of sampling points. The current signal sequence $x_2(n)$ is subjected to windowing processing, with a window size of K and the number of windows is s . The difference window is constructed to eliminate the same noise components contained in adjacent window signals. The definition of the difference window is as follows:

$$h^j = \sum_{i=jK+1}^{(j+1)K} x_2^{j+1}(i) - \sum_{i=(j-1)K+1}^{jK} x_2^j(i), \quad 1 \leq j < s \quad (8)$$

Among them, h^j represents the j th difference window.

After constructing the difference window, calculate the mean of the difference window to smooth the effect of residual noise and obtain the central tendency of the current signal within the window, in order to better describe the overall feature of the arc fault current within the window. As shown in Eq. (9):

$$z^j = \frac{\sum h^j}{K}, \quad 1 \leq j < s \quad (9)$$

Since the current signal undergoes a significant decline when an arc fault occurs, the mean of the difference window between the fault occurrence window and the preceding window will be the smallest and negative, while the mean of the difference window between the subsequent window and the fault occurrence window will be the largest. Therefore, the position J of the fault occurrence window is defined as follows:

$$J = \{J | z^{J-1} = \min(z^j), z^J = \max(z^j)\} \quad (10)$$

Subsequently, an absolute value method is applied to process the mean of the difference window to eliminate its directional nature, and the maximum value is selected as the feature value of the arc fault current signal $x_2(n)$, achieve an effective representation of the arc fault features.

$$S_1 = \max(|z^j|), \quad 1 \leq j < s \quad (11)$$

The transient feature extraction method based on AWD has located the fault occurrence window position, effectively extracting the transient change feature of the photovoltaic DC arc fault current signal, avoiding the issue of insufficient feature representation when extracting features from the overall current signal, and is conducive to the rapid detection of arc faults. However, changes in system load cause the trend of line current waveform changes to be similar to the arc initiation waveform, relying solely on AWD feature is prone to causing misjudgment.

3.2. Steady-state feature extraction based on ED

In response to the system load changes that cause the current waveform trend to be similar to the arc initiation waveform, the issue that using only AWD feature is prone to causing misjudgment, this paper designs a steady-state feature description method based on ED. Based on the division of windows and the positioning of the fault occurrence window, select the normal window with the smallest variance before the fault occurrence window and the fault window with the largest variance after the fault occurrence window, use the CEEMDAN algorithm [22,23] to decompose the window signal, calculate the spectral kurtosis of each modal component [24] and select the component with the largest spectral kurtosis as the optimal component, by calculating the energy difference of the window signal, capture the energy changes produced during the arc burning process, achieve the significant expression of the steady-state ED feature. The specific steps are as follows:

For the normal signal $x_1(n)$, select the window with the smallest variance to construct signal y_1^1 , representing a more stable normal signal with less interference. And select the window with the largest variance to construct signal y_1^2 , representing a normal signal with poorer stability and more interference. The definitions are as follows:

$$y_1^1 = \{x_1^j | \sigma_j^2 = \min\{\sigma_1^2, \sigma_2^2, \dots, \sigma_s^2\}\}, 1 \leq j \leq s \quad (12)$$

$$y_1^2 = \{x_1^j | \sigma_j^2 = \max\{\sigma_1^2, \sigma_2^2, \dots, \sigma_s^2\}\}, 1 \leq j \leq s \quad (13)$$

For the arc fault signal $x_2(n)$, let the fault occurrence window be the J th window. Select the window with the smallest variance before the fault occurrence window to construct signal y_2^1 , representing a more stable normal signal with less interference. And select the window with the largest variance after the fault occurrence window to construct signal y_2^2 , representing an unstable fault signal with more interference. The definitions are as follows:

$$y_2^1 = \{x_2^j | \sigma_j^2 = \min\{\sigma_1^2, \sigma_2^2, \dots, \sigma_{J-1}^2\}\}, 1 \leq j < J \quad (14)$$

$$y_2^2 = \{x_2^j | \sigma_j^2 = \max\{\sigma_{J+1}^2, \sigma_{J+2}^2, \dots, \sigma_s^2\}\}, J < j \leq s \quad (15)$$

Subsequently, the signal is decomposed by using the CEEMDAN method, as shown in Eq. (16). The CEEMDAN algorithm effectively eliminates the problem of modal aliasing by adaptively adjusting the noise level and optimizing the decomposition process, providing more accurate and stable decomposition results.

$$y(n) = \sum_{i=1}^f IMF_i(n) + R(n) \quad (16)$$

Here, $IMF_i(n)$ represents the i th modal component, f is the total number of modal components, $R(n)$ is the residual component obtained from the decomposition.

Subsequently, calculate the spectral kurtosis values of each modal component, which are used to measure the steepness of the modal component's spectrum, and is defined as follows:

$$Q = \frac{(\sum (PSD(k)^2 * k^4)) * (\sum (PSD(k)^2))}{(\sum (PSD(k)^2 * k^2))^2} \quad (17)$$

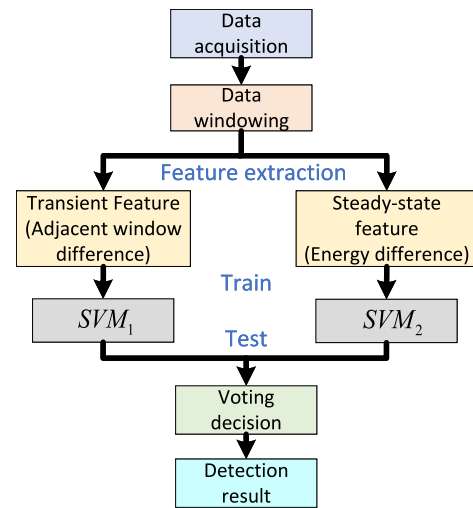


Fig. 2. Dc arc fault detection process based on SVM.

$$PSD(k) = \frac{|F(IMF(n))|^2}{N} \quad (18)$$

Among them, the modal component with the highest spectral kurtosis value appears more concentrated in the spectrum, with a sharper spectral peak, suggesting that this modal component contains more effective components. Therefore, the modal component with the highest spectral kurtosis value is selected as the optimal component.

Finally, calculate the signal ED feature, as shown in Eq. (19):

$$S_2 = E_2 - E_1 \quad (19)$$

Here, E_2 represents the energy of the optimal modal component of signal y_2^2 , E_1 represents the energy of the optimal modal component of signal y_1^1 .

The steady-state feature extraction method based on ED achieves a significant description of the steady-state feature during the arc burning process. It addresses the issue of misjudgment that arises from using transient feature for arc fault detection. This method provides a new perspective and solution for accurate arc fault detection, significantly enhancing the reliability of arc fault detection.

4. Voting decision based on support vector machine

This paper proposes a novel feature extraction method for arc fault current. Based on arc characteristics, the arc occurrence process is divided into transient and steady-state processes. The original arc fault current signal undergoes windowing, transient feature extraction, and steady-state feature extraction to achieve a comprehensive expression of arc fault current features. Based on this, this paper selects SVM for arc fault detection [25,26]. As a powerful binary classifier, SVM has strong generalization ability and robustness, making it highly suitable for effective arc fault detection. The experimental data is labeled and divided into training and testing sets. Feature extraction is performed according to the aforementioned steps for training and testing models SVM_1 and SVM_2 . Finally, a voting decision is made [27], when both transient and steady-state features match the fault features, it is determined that there is an arc fault. The process is shown in Fig. 2.

5. Experimental analysis

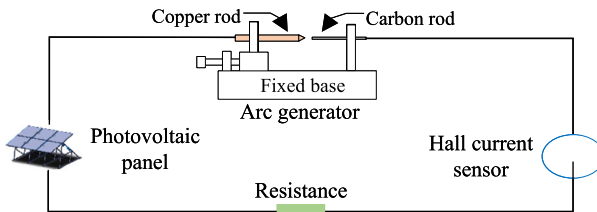


Fig. 3. Schematic diagram of DC series arc fault experiment.

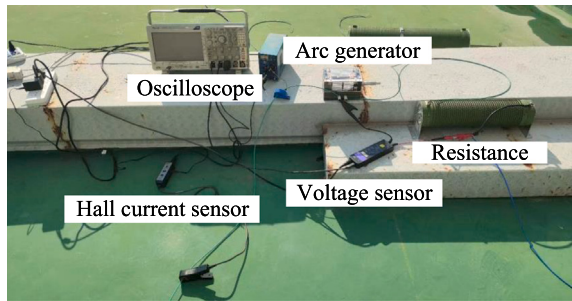


Fig. 4. Circuit of DC series arc fault experiment.

Table 1
The composition of the collected experimental data.

Load \ Current level	Type	Arc gap			Normal
		0.5 mm	1.0 mm	1.5 mm	
Resistance box	3 A	6	6	6	18
	5 A	6	6	6	18
	10 A	6	6	6	18
	15 A	6	6	6	18
	30 A	6	6	6	18
	Resistance:12 Ω	3 A	2	2	12
Resistance:24 Ω	6 A	2	2	2	12
	3 A	2	2	2	12
	6 A	2	2	2	12
	3 A	2	2	2	12
Resistance:48 Ω	6 A	2	2	2	12

5.1. Experimental platform construction and data collection experiment

This paper builds an experimental circuit for photovoltaic DC series arc fault detection based on the standard UL1699B [28], with the schematic diagram shown in Fig. 3, mainly consisting of four parts: photovoltaic panels, arc generator, hall current sensor, and load. The constructed experimental circuit is shown in Fig. 4. The arc generator selected is a drawn-arc type arc generator, using a Hall current sensor to collect current signals, using an oscilloscope for observation, with a sampling rate of 500 kSa/s, a signal sampling duration of 1 s, and a total of 500,000 signal sampling points. Among them, UL1699B requires detection within two seconds after the arc occurs, thus setting the signal sampling duration to 1 s complies with the standard.

During the experimental data collection process, comprehensively considered the effects of changes in line current levels, arc gaps, and load resistances, experiments were designed for different line current levels of 3 A, 5 A, 10 A, 15 A, and 30 A, experiments were designed for different arc gaps of 0.5 mm, 1.0 mm, and 1.5 mm, and experiments were designed for different resistance sizes of 12, 24, and 48 ohms. A total of 162 sets of normal current data and 126 sets of arc fault current data were collected in the experiments, the composition of the experimental data is shown in Table 1. Fig. 5 shows some arc fault current signal waveforms under different current levels, different arc gaps, and different resistance sizes.

As shown in Fig. 5(a), the current level affects the electric field intensity, which in turn influences the stability of the arc. When the

current level is 3 A, the electric field intensity is low and unevenly distributed, preventing the arc from forming a stable plasma channel, resulting in significant fluctuations in the current signal. As the current increases to 5 A, 10 A, and 15 A, the electric field intensity increases and becomes more evenly distributed, leading to a higher electron density. This allows the arc to form a stable plasma channel, reducing current fluctuations. However, when the current level further increases to 30 A, the rise in electric field intensity results in a higher collision frequency between electrons and ions in the plasma, generating more heat and thus affecting the plasma's stability, leading to increased current fluctuations. In Fig. 5(b), the arc gap affects the length of the arc, thereby influencing the arc's stability. When the arc gap is 0.5 mm, the smaller gap helps maintain a higher electron density, increasing the plasma's conductivity and providing a stable conduction path for the arc, resulting in smaller current fluctuations. As the arc gap increases to 1.0 mm and 1.5 mm, the arc becomes longer, and the path of electron and ion movement within the arc extends, causing uneven distribution of electron and ion density within the plasma. This affects the stability of the arc and results in larger current fluctuations. In Fig. 5(c), high resistance limits the flow of current, thereby exerting a suppressive effect on the arc. When the resistance is 12Ω, the resistance is relatively low, allowing electrons and ions to maintain relatively high speeds and kinetic energy, increasing the collision frequency and resulting in larger current fluctuations. As the resistance increases, electrons and ions lose more kinetic energy when passing through the resistance, causing their speeds in the arc to decrease. This reduces the collision frequency, leading to a gradual stabilization of the current waveform.

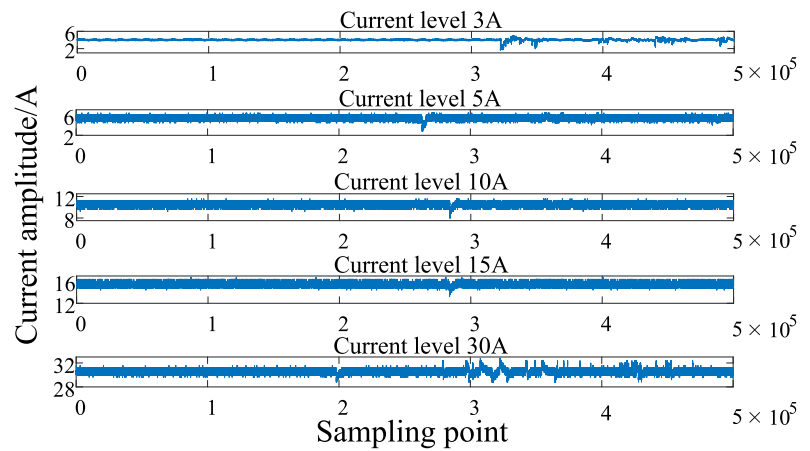
5.2. Signal windowing experiment based on autocorrelation function

DC signals are non-periodic, highly random, and non-stationary, making it impossible to directly segment them for processing. This paper first employs the autocorrelation function method to process the normal current signal, with the results shown in Fig. 6.

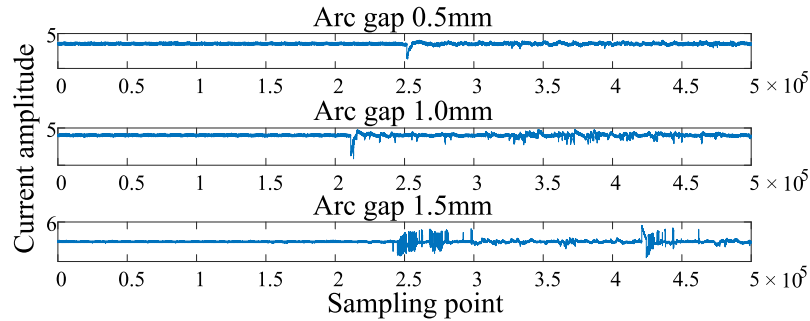
Experimental results show that, within this dataset, the autocorrelation function windowing method can capture the repetitive pattern in the DC current signal, manifest as periodicity in the autocorrelation function. Analyzing this periodic pattern is closely related to the photovoltaic power supply equipment used in the experiment. Under different current levels and resistance sizes, the autocorrelation function of the normal current signal exhibits a consistent periodic trend. Due to the high randomness of DC signals, the autocorrelation coefficients are generally low. When using a resistance box as the load, the autocorrelation function waveform of the normal current signal shows almost no difference across different current levels, indicating that the current level has a minimal effect. However, when resistance is used as the load, the periodic features of the autocorrelation function waveform of the normal current signal are weakened as the resistance size increases. This is because increasing the resistance size leads to a higher damping coefficient in the circuit system, affecting the oscillatory behavior of the signal and thereby impacting the periodicity of the autocorrelation function of the normal current signal.

When selecting the window size, two factors need to be considered. On one hand, the window size K must meet the requirements for periodicity and peak positions as specified in the definition. On the other hand, the window size K must satisfy the constraint of being divisible by the total number of data sample points. Thus, the window size $K = 10000$ was selected. Subsequently, the mean and variance of the normal current signal and its segmented window signals were calculated, and the error was computed by using Eq. (7), as shown in Fig. 7.

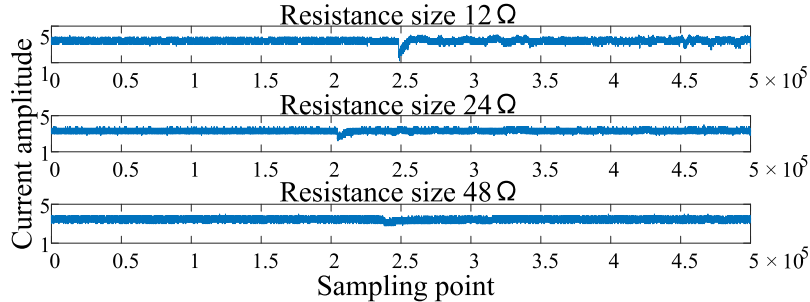
Observations indicate that when the window size $K = 10000$ is selected, the windowing verification error for normal current signals at different current levels and resistance sizes is very small, close to zero, and the overall trend shows consistent stability. The smaller the value of err , the more it indicates that there are no anomalies in the statistical features of the signals within the windows. Therefore, it can be concluded that the setting of the window size $K = 10000$ is reasonable.



(a) Arc fault current signal waveform under different current levels when the arc gap is 1.0mm.



(b) Arc fault current signal waveform under different arc gaps when the current level is 3A.



(c) Arc fault current signal waveform under different resistance sizes when the current level is 3A and the arc gap is 1.0mm.

Fig. 5. Arc fault current signal waveform.

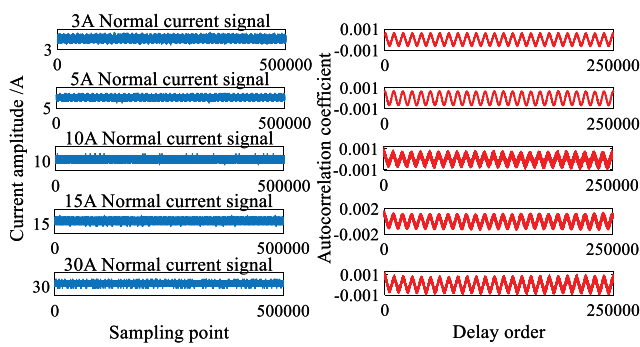
5.3. Arc fault stage feature extraction experiment

5.3.1. Optimal window size verification experiment

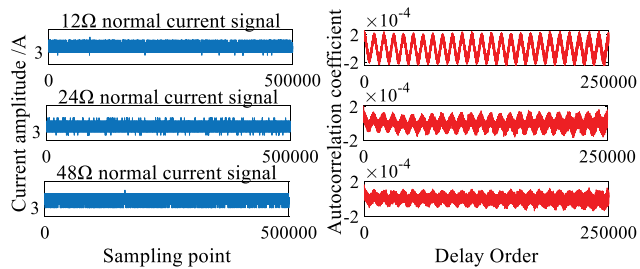
The purpose of signal windowing is to better capture the transient feature of the signal. In order to verify that the window size determined by the autocorrelation function windowing method proposed in this paper is the optimal choice, the window sizes such as $K = 5000$, $K = 20000$ and $K = 50000$ are subjectively selected to extract AWD feature, and the results are shown in Fig. 8.

Observing Fig. 8, it can be found that when the window size is $K = 5000$ and $K = 50000$, there is an overlap in AWD feature values between normal current signals and arc fault current signals, indicating that the differentiation effect of AWD feature is not ideal when the window size is $K = 5000$ and $K = 50000$. The main reason is that when the window size is $K = 5000$, the window is too small, leading

to an inability to accurately express the features of arc fault current signals, resulting in feature loss. When the window size is $K = 50000$, the window is too large, causing some arc fault current features to be insufficiently expressed, making it difficult to accurately capture the change feature of the arc fault. When the window size is $K = 20000$, it can be seen that although there is no overlap in AWD feature values between normal current signals and arc fault current signals, a clear threshold dividing line has not been formed, and the differentiation effect remains insufficient. The window size of $K = 10000$ determined by the autocorrelation function windowing method proposed in this paper, can effectively distinguish between normal and arc fault signals. AWD feature values form a clear threshold dividing line, yielding the best segmentation effect.

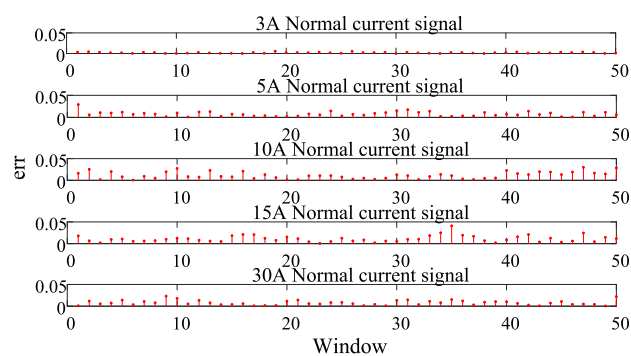


(a) Normal current signals and its autocorrelation function results under different current levels.

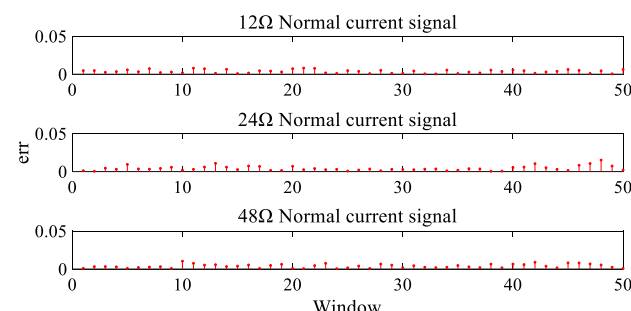


(b) Normal current signals and its autocorrelation function results under different resistance sizes.

Fig. 6. Normal current signals and its autocorrelation function results.



(a) Verification error of normal current signals windowing under different current levels.



(b) Verification error of normal current signals windowing under different resistance sizes.

Fig. 7. Verification error of normal current signals windowing.

5.3.2. Transient feature extraction experiment based on AWD

Taking an arc fault current signal with a load of a set of resistance box, a current level of 3 A, and an arc gap of 0.5 mm as an example, with a sampling point of 500,000. The window size $K = 10,000$ was determined by using the autocorrelation function windowing method, which divided the signal into 50 independent windows. When performing difference analysis on these windows, 49 difference windows were constructed, and the mean values of the difference windows were calculated. By identifying two key pieces of window information: the mean value of the 27th difference window was the minimum, and the mean value of the 28th difference window was the maximum. It could be concluded that the fault occurrence window position corresponded to the 28th window of the original signal. Subsequently, the mean values of the difference windows were processed with absolute values to eliminate directional bias. Finally, the maximum value was selected as the feature value of this group of signals.

Follow the aforementioned steps, the transient feature extraction based on AWD was performed for both normal current signals and arc fault current signals, and the distribution of AWD features of some current signals is shown in Fig. 9.

The experimental results show that:

(1) Fig. 9(a) illustrates the distribution of AWD feature values under different current levels and arc gaps when the load is a resistance box. The trend observed from the figure indicates that as the current level increases, AWD feature values initially decrease and then increase. At a current of 3 A, the electric field strength between the electrodes is low, insufficient to effectively ionize the gas. This results in poor arc stability and significant fluctuation during arc initiation, leading to larger AWD feature values. As the current increases, the electric field strength also increases, facilitating arc ionization and maintenance. The enhanced plasma stability reduces fluctuations during arc initiation, thereby decreasing AWD feature values. However, when the current further increases to 30 A, the plasma undergoes rapid energy release and reorganization, causing increased fluctuations at the moment of arc initiation, which results in larger AWD feature values.

(2) Fig. 9(b) illustrates the distribution of AWD feature values under different resistance sizes and arc gaps when the load is a resistance and the current level is 6 A. After an arc fault occurs, when the resistance is 12Ω , the smaller resistance means that less energy is converted into heat, and more energy is used for the ionization process and maintaining the arc. This leads to rapid movement of electrons and ions, increasing the fluctuations at the moment of arc initiation and resulting in larger AWD feature values. As the resistance size increases, more energy is dissipated as heat across the resistance, reducing the energy available for ionization and maintaining the arc. This suppresses arc development, leading to decreased fluctuations at the moment of arc initiation and smaller AWD feature values.

(3) From the analysis of Figs. 9(a) and 9(b), it can be concluded that when the arc gap is 0.5 mm, the small gap results in a higher plasma density within the arc channel. This high density supports stable arc development and results in smaller fluctuations at the moment of arc initiation, leading to smaller AWD feature values. As the arc gap increases, the arc shape becomes more diffuse, leading to a decrease in plasma density. This results in increased fluctuations at the moment of arc initiation and larger AWD feature values.

Based on the above analysis, AWD feature can effectively capture the transient fluctuation feature caused by arc faults during arc initiation, achieving the distinction between normal line current and arc fault current signals. However, relying solely on AWD feature cannot meet the detection requirements for arc faults under all influencing factors. Therefore, on the basis of extracting AWD feature, this paper further extracts the steady-state feature of the arc burning in the arc fault current, comprehensively considering the diversity of arc fault features.

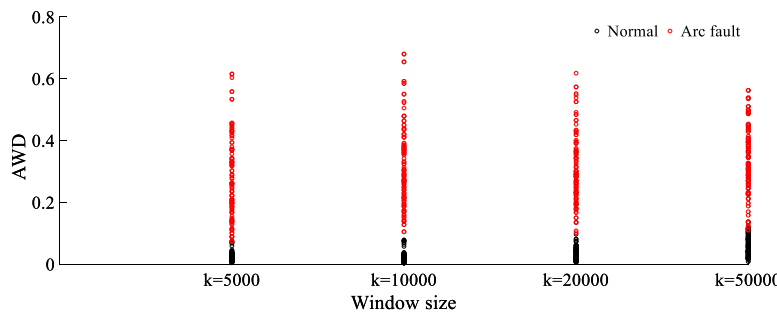
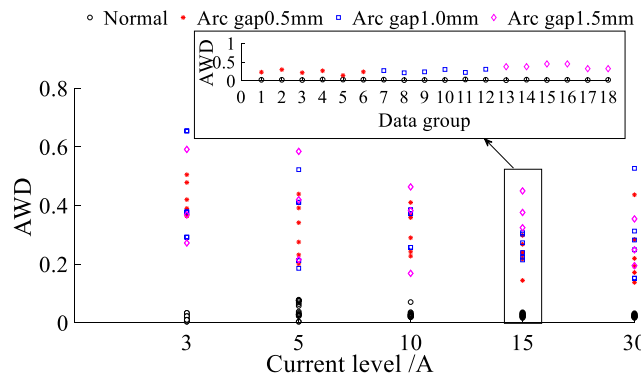
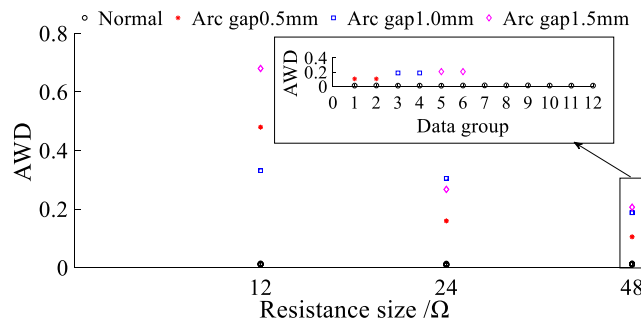


Fig. 8. Distribution of AWD feature values under different window sizes.



(a) Distribution of AWD feature values under different current levels and arc gaps.



(b) Distribution of AWD feature values under different resistance sizes and arc gaps.

Fig. 9. Distribution of AWD feature values under different influencing factors.

5.3.3. Steady-state feature extraction experiment based on ED

Selecting an arc fault current signal with a load of a set of resistance boxes, a current level of 3 A, and an arc gap of 0.5 mm. The window with the smallest difference before the fault occurrence was chosen, as well as the window with the largest difference after the fault occurrence window, for CEEMDAN decomposition, as shown in Fig. 10.

As can be seen from Fig. 10, the normal window signal was decomposed into 14 IMF components, and the fault window signal was decomposed into 15 IMF components. The decomposition results had good completeness and overcame the modal aliasing problem. The spectral kurtosis index was calculated for all IMF components, the spectral kurtosis values corresponding to each IMF component of the normal window signal were [1.16, 1.14, 1.22, 1.13, 1.12, 1.10, 1.12, 1.18, 1.00, 1.00, 1.21, 1.16, 1.53, 1.15, 1.00], the spectral kurtosis values corresponding to each IMF component of the fault window signal were

[1.14, 1.25, 1.92, 1.44, 1.41, 1.40, 1.27, 1.16, 1.07, 1.14, 1.06, 1.66, 1.75, 4.82, 1.00]. Therefore, for the normal window signal, IMF12 was selected as the optimal component, and for the fault window signal, IMF14 was selected as the optimal component. Then the energy spectral density of the optimal components was compared, as shown in Fig. 11.

Clearly, the optimal components selected through the spectral kurtosis index exhibit steeper spectral features, and the frequency distribution is more concentrated. During the normal phase, the energy spectral density of the signal is much lower than the energy spectral density during fault occurrence, effectively highlighting the significant changes in the fault window signal.

ED feature extraction was performed on normal current signals and arc fault current signals, and the distribution of ED features of some current signals is shown in Fig. 12.

The experimental results show that:

(1) Fig. 12(a) illustrates the distribution of ED feature values under different current levels and arc gap conditions when the load is a resistance box. As the current level increases, the ED feature values distribution initially decreases and then increases. This occurs because, at a current level of 3 A, the electric field strength is low, making the arc plasma state unstable and susceptible to external influences, leading to a higher amount of interference components and, consequently, larger ED feature values. As the current level increases, the electric field strength also increases, improving the stability of the plasma and reducing the generation of interference components, which is reflected as a decrease in ED feature values. However, as the current level continues to increase, the thermal and radiation effects of the arc become significantly stronger, leading to more interference components and an increase in ED feature values.

(2) Fig. 12(b) illustrates the distribution of ED feature values under different resistance sizes and arc gaps when the load is a resistance and the current level is 6 A. After an arc fault occurs, the ED feature values is larger when the resistance is 12Ω . However, as the resistance increases, the ED feature values shows a decreasing trend. The primary reason is that as the resistance increases, the damping effect of the arc is enhanced, leading to plasma attenuation, reducing the generation of frequency components and then decreasing the ED feature values.

(3) Analyzing Figs. 12(a) and 12(b), it can be observed that the ED feature values are smaller with an arc gap of 0.5 mm and larger with a gap of 1.5 mm. This indicates that as the arc gap increases, the ED feature values tend to increase. The reason is that as the arc gap increases, the arc length also increases, leading to a higher arc voltage. This results in a rise in arc temperature, increasing thermal radiation and conduction of the arc, causing interference in the current signal's frequency components and leading to larger ED feature values.

Based on the analysis, compared with arc fault current signals, the ED feature values of normal current signals are smaller. The main reason is that the circuit conditions generating normal current signals are more stable, with less interference and no involvement of arc discharge events, showing a strong overall stability in the signal. The

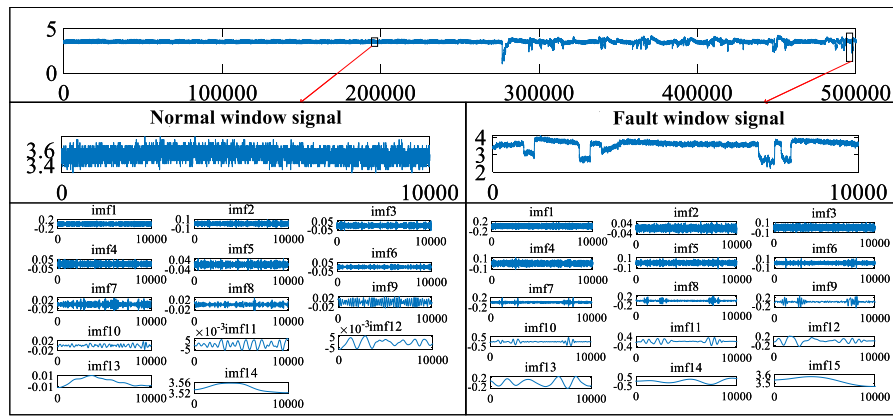


Fig. 10. Arc fault current waveform and the selected window signals with its decomposition results.

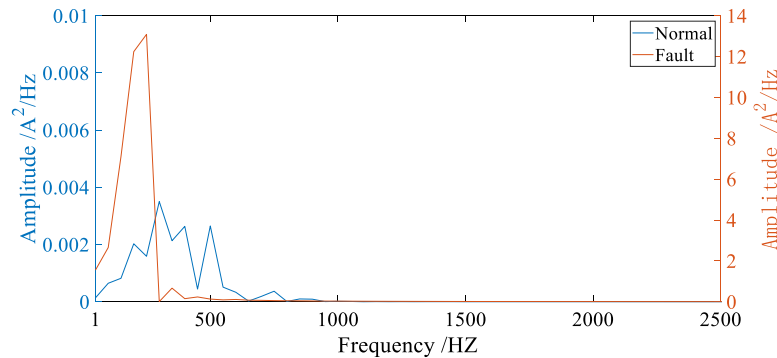


Fig. 11. Comparison of energy spectral density of optimal component.

Table 2
Model accuracy, decision accuracy, false positive rate, and false negative rate under different ratios.

$M_1 : M_2$	Model accuracy	Decision accuracy	False positive rate	False negative rate
5:5	99.51%	98.54%	0%	1.46%
	99.03%			
6:4	99.57%	99.48%	0%	0.52%
	99.91%			
7:3	99.77%	99.77%	0%	0.23%
	100%			

ED feature can capture the differences between arc fault current signals and normal current signals, achieving a significant expression of the steady-state feature of arc fault current signals, providing a reliable basis for distinguishing between normal current signals and arc fault current signals.

5.4. Voting decision experiment based on support vector machine

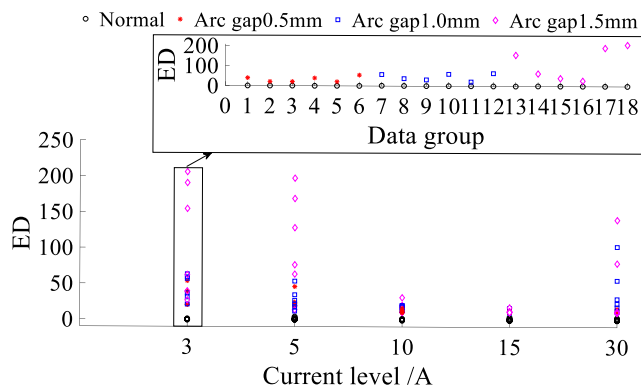
In the arc fault detection experiment based on the SVM model, the SVM model selected the RBF kernel function, with the penalty factor set to 0.5 and the width parameter set to 10. The experiment included three scenarios with different training set M_1 to test set M_2 ratios: 5:5, 6:4, and 7:3, to comprehensively evaluate the performance of the SVM model under varying ratios. The effectiveness of the proposed method was measured using decision accuracy, false positive rate, and false negative rate as indicators. A 10-fold cross-validation was used in the experiment, with the average value as the evaluation metric. Table 2 details the model accuracy, decision accuracy, false positive rate, and false negative rate under different ratios.

Among Table 2, decision accuracy represents the system's ability to correctly identify fault and normal signals. High accuracy indicates that the system is reliable and capable of providing accurate judgments.

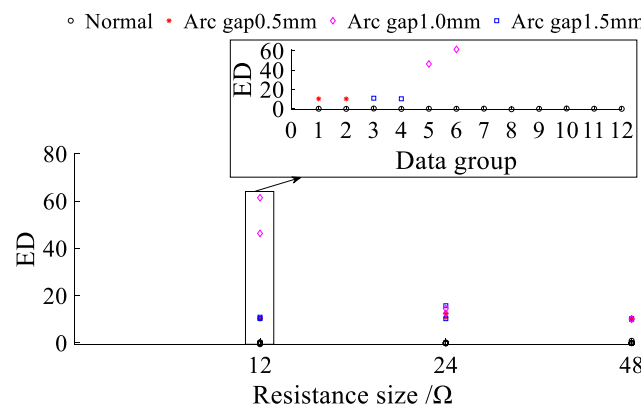
The false positive rate represents the proportion of normal signals incorrectly identified as fault signals. A false positive rate of 0 means the system can accurately identify all normal signals without error. The false negative rate refers to the proportion of fault signals that the system fails to identify. A lower false negative rate indicates that the system can capture nearly all fault signals, allowing for timely intervention to prevent potential risks.

Based on the data analysis from Table 2, the SVM_1 and SVM_2 models have a high accuracy rate, the voting decision effect is good, avoiding misjudgment and having a low false negative rate. As the amount of training data increases, the model training effect is improved, which not only enhances the model's performance, as reflected in the increase in model accuracy, but also improves decision accuracy, and reduces the possibility of missing a fault. Under different proportions of data set division, and in multiple random divisions of the data set under the same proportion, SVM has shown high stability and excellent performance, fully proving its outstanding robustness and adaptability.

Furthermore, to verify that SVM (RBF kernel) is the optimal choice, comparative experiments were conducted by using SVM (linear kernel) and SVM (second-order polynomial kernel). The ratio of the training set to the testing set was set to 7:3, using decision accuracy and runtime



(a) Distribution of ED feature values under different current levels and arc gaps.



(b) Distribution of ED feature values under different resistance sizes and arc gaps.

Fig. 12. Distribution of ED feature values under different influencing factors.

Table 3

Decision accuracy and running time of SVM with different kernel functions.

Model	Decision accuracy	Run time (s)
SVM (Linear kernel)	95.7%	0.0110534
SVM (second order polynomial kernel)	98.84%	0.012038
SVM (RBF kernel)	99.77%	0.0088192

as evaluation metrics, with the experimental results being the average of 10 cross-validations, as shown in Table 3.

According to the content of Table 3, SVM demonstrates good performance when using all three kernels. However, the decision accuracy of SVM (linear kernel) is relatively lower than that of the other two cases, primarily because there are linearly inseparable sample points in the feature set, which the linear kernel cannot effectively distinguish. Although SVM (second-order polynomial kernel) can handle nonlinear problems, its nonlinear mapping capability is relatively limited, and the model complexity is comparatively high. Compared to SVM (RBF kernel), SVM (second-order polynomial kernel) has a relatively lower accuracy and longer runtime. SVM (RBF kernel) can adaptively find suitable decision boundaries through Gaussian distribution mapping, flexibly handling various nonlinear distributions. In summary, SVM (RBF kernel) can capture the nonlinear features of the data more flexibly and accurately, yielding the best performance.

5.5. Comparison with other photovoltaic DC series arc fault detection methods

To validate the effectiveness of the proposed method, we selected methods from Refs. [13–18] and conducted experiments based on a self-constructed dataset. The proposed method achieved the best detection performance when the training set to test set ratio was 7:3. Therefore, under the same test set size, methods from Refs. [13–18] were selected for comparative experiments. The results are shown in Table 4.

The experimental results show that:

(1) In terms of feature extraction, Ref. [13] employs segmented feature extraction from signals, which better describes the time-domain fluctuation features of arc fault currents. The feature extraction methods used in Refs. [14–18] extract features from the signal as a whole, which can lead to information redundancy, weaken feature representation, and result in the loss of key feature information. The methods proposed in Refs. [13,15], and [16] focus only on single aspects of arc fault features extraction for detection, while the features of arc faults are complex and diverse. Thus, these methods lack representational adequacy. The methods in Refs. [14,17], and [18] extract features from multiple domains, including both time and frequency, considering the diversity of arc features. However, the extracted features are susceptible to interference from external environmental and circuit factors, leading to poor generalizability of these methods.

(2) In terms of detection, Refs. [13–18] all use the threshold method to determine whether an arc fault has occurred, and the selection of the threshold faces the challenge of the complexity and diversity of the signals, and is also subject to interference from external environmental factors, which to some extent affects the accuracy and reliability of arc fault detection.

(3) In terms of detection accuracy, the method proposed in Ref. [14] uses a standard deviation feature extracted from the entire signal. However, the current signal collected in this study contains 500,000 sampling points, causing the extracted standard deviation feature to inadequately represent arc fault features, which results in poor detection performance. The methods in Refs. [15–17], and [18] choose to extract the frequency domain features of arc fault currents in the high-frequency range. However, because the self-constructed dataset uses resistances as the load, it lacks high-frequency electronic components such as inverters. Additionally, the resistance, overall circuit, and the mechanism and physical characteristics of DC arc generation affect the collected arc fault current signals, resulting in more pronounced fault frequency components in the low-frequency range and lower distinguishability in the high-frequency range. Therefore, these methods perform poorly on the self-constructed dataset in this paper. The method proposed in Ref. [13] shows higher accuracy. The main reason is that the proposed rate of change of periodic mean feature is extracted based on changes in adjacent windows, accurately capturing waveform changes caused by arc faults. However, this method cannot accurately distinguish waveform fluctuations caused by load changes.

In summary, the two-stage feature comprehensive decision method proposed in this paper, specifically extracts the transient feature of arc initiation and the steady-state feature of arc burning, achieving a comprehensive expression of the features during the arc occurrence process. Using SVM instead of the traditional threshold method for arc fault detection demonstrates superior detection performance, and the use of voting decision method enhances the reliability of arc fault detection.

6. Conclusion

This paper proposes a photovoltaic DC series arc fault detection method based on two-stage feature comprehensive decision. The proposed autocorrelation function windowing method addresses the difficulty in determining the window size due to the non-periodic and

Table 4
Comparative experimental results.

Method	Parameter setting	Detection result
Ref. [13]	Feature threshold : 0.02	91.16%
Ref. [14]	Feature threshold of standard deviation : 0.28	60.12%
	Feature threshold of frequency band energy : 0.2	
Ref. [15]	Feature threshold : 0.002	59.54%
Ref. [16]	Feature threshold : 1	58.95%
Ref. [17]	Feature threshold of mean change : 0.11	56.05%
	Feature threshold of frequency band energy : 350	
Ref. [18]	Feature threshold of high frequency signal maximum : 1.3	57.2%
	Feature threshold of wavelet detail coefficient variance : 0.07	
	Feature threshold of wavelet detail coefficient modular maxima : 1.2	
Our work	Penalty factor 0.5, width parameter 10	99.77%

random nature of DC arcs. Based on the transient characteristics of arc initiation stage and the steady-state characteristics of arc burning stage, the whole arc process is divided into transient and steady-state processes. A transient feature description of AWD is further proposed to locate the fault occurrence window and extract the transient fluctuation feature of the arc fault. To avoid misjudgments in arc faults by relying solely on transient feature, a steady-state feature description of ED is proposed. By selecting the window with the smallest variance before the fault occurrence and the window with the largest variance after the fault occurrence, the CEEMDAN algorithm combined with spectral kurtosis is used to select the optimal component for calculating energy differences. This approach achieves a significant representation of steady-state feature information of arc faults. Finally, SVM and voting decision method are used to achieve series arc fault detection, significantly improving the accuracy and reliability of arc fault detection.

In the future research work, based on the detection algorithm proposed in this paper, efficient and reliable communication technology and management analysis software can be comprehensively used to design a multi-point detection method for actual photovoltaic systems, so as to improve the intelligent level of arc fault detection in actual photovoltaic systems.

CRediT authorship contribution statement

Bangzheng Han: Writing – review & editing, Writing – original draft. **Guofeng Zou:** Writing – review & editing. **Wei Wang:** Writing – review & editing. **Jinjie Li:** Writing – review & editing. **Xiaofei Zhang:** Writing – review & editing.

Declaration of competing interest

The authors declare the following financial interests/personal relationships which may be considered as potential competing interests: Guofeng Zou reports financial support was provided by The Natural Science Foundation of Shandong Province (ZR2022MF307). Guofeng Zou reports financial support was provided by The National Natural Science Foundation of China (52077221). If there are other authors, they declare that they have no known competing financial interests or personal relationships that could have appeared to influence the work reported in this paper.

Acknowledgments

The study in this article was sponsored by the Natural Science Foundation of Shandong Province, China (ZR2022MF307), the National Natural Science Foundation of China (52077221).

References

- [1] B. Hu, B. Ye, X. Wang, L. Dai, Y. Chen, M. Zhang, Low carbon economic dispatching for power system integrated with large scale photovoltaic power generation, in: 2017 IEEE Conference on Energy Internet and Energy System Integration (EI2), IEEE, 2017, pp. 1–6.
- [2] J.L. Putzke, F.M. Bayer, A.M. Jaime, C.A. Haab, L.V. Bellinaso, L. Michels, Methodology for predicting the self-extinction of standardized arc faults in photovoltaic systems, *Sol. Energy* 278 (2024) 112714.
- [3] L. Lin, W. Gao, G. Yang, A DC arc fault location method for PV systems based on redundant antenna array and ellipse algorithm, *Sol. Energy* 274 (2024) 112588.
- [4] W. Gao, R.-J. Wai, Series arc fault detection of grid-connected PV system via svd denoising and IEWT-TWSVM, *IEEE J. Photovolt.* 11 (6) (2021) 1493–1510.
- [5] H. Qian, B. Lee, Z. Wu, G. Wang, Research on DC arc fault detection in PV systems based on adjacent multi-segment spectral similarity and adaptive threshold model, *Sol. Energy* 264 (2023) 112011.
- [6] Q. Xiong, S. Ji, X. Liu, X. Feng, F. Zhang, L. Zhu, A.L. Gattozzi, R.E. Hebner, Detecting and localizing series arc fault in photovoltaic systems based on time and frequency characteristics of capacitor current, *Sol. Energy* 170 (2018) 788–799.
- [7] S. Zhao, Y. Wang, F. Niu, C. Zhu, Y. Xu, K. Li, A series DC arc fault detection method based on steady pattern of high-frequency electromagnetic radiation, *IEEE Trans. Plasma Sci.* 47 (9) (2019) 4370–4377.
- [8] W. Miao, X. Liu, K. Lam, P.W. Pong, Arc-faults detection in PV systems by measuring pink noise with magnetic sensors, *IEEE Trans. Magn.* 55 (7) (2019) 1–6.
- [9] Q. Xiong, S. Ji, L. Zhu, L. Zhong, Y. Liu, A novel DC arc fault detection method based on electromagnetic radiation signal, *IEEE Trans. Plasma Sci.* 45 (3) (2017) 472–478.
- [10] S. Navalpakkam Ananthan, X. Feng, C. Penney, A. Gattozzi, R. Hebner, S. Santoso, Voltage differential protection for series arc fault detection in low-voltage DC systems, *Inventions* 6 (1) (2020) 5.
- [11] A. Shekhar, L. Ramirez-Elizondo, S. Bandyopadhyay, L. Mackay, P. Bauera, Detection of series arcs using load side voltage drop for protection of low voltage DC systems, *IEEE Trans. Smart Grid* 9 (6) (2017) 6288–6297.
- [12] Q. Lu, Z. Ye, M. Su, Y. Li, Y. Sun, H. Huang, A DC series arc fault detection method using line current and supply voltage, *IEEE Access* 8 (2020) 10134–10146.
- [13] G. Zhang, C. Li, Y. Zhao, B. Liu, L. Li, Series DC arcing fault detection method based on rate of cycle mean, *J. Electr. Eng.* 11 (09) (2019) 44–47.
- [14] C. Wu, W. Xu, Z. Li, L. Xu, Are fault type identification and circuit protection in photovoltaic system, *Proc. CSEE* 37 (17) (2017) 5028–5036.
- [15] Y. Wang, Y. Li, L. Ge, F. Niu, K. Li, A series DC arcing fault recognition method based on sliding discrete Fourier transform, *Trans. China Electrotech. Soc.* 32 (19) (2017) 118–124.
- [16] Z. Di, Q. Xiong, C. Zhang, R. Li, S. Ji, DC Arc fault detection method based on weighted differential current, *J. Xi 'an Jiaotong Univ.* 56 (05) (2022) 141–148.
- [17] G. Zhang, D. Yang, S. Ji, H. Li, Research on photovoltaic system series DC Arc fault detection, *J. Power Supply* 19 (1) (2021) 90–96.
- [18] L. Mu, Y. Wang, W. Jiang, F. Zhang, Study on characteristics and detection method of DC arc fault for photovoltaic system, in: Proceedings of the CSEE, Vol. 36, 2016, pp. 5236–5244.
- [19] H. Yuejie, Z. Diqing, A method of PV arc fault detection in time-frequency domain, *Low Volt. Appar.* (10) (2018) 25.
- [20] H. Jixin, X. Yongxin, G. Yicheng, W. Yongqiang, A multi-feature fusion-based method to recognize series DC Arc fault in photovoltaic system, *Mod. Electr. Power* 39 (5) (2022) 529–536.
- [21] X. Huang, C. Wu, Z. Li, F. Wang, Comparative study of DC arc fault detection methods in photovoltaic systems, *Acta Energ. Sol. Sin.* 41 (8) (2020) 204–214.
- [22] S. Tian, X. Bian, Z. Tang, K. Yang, L. Li, Fault diagnosis of gas pressure regulators based on CEEMDAN and feature clustering, *IEEE Access* 7 (2019) 132492–132502.

- [23] J. Wu, W. Wang, T. Shang, J. Cao, A novel series arc fault detection method based on CEEMDAN and IFAW-1DCNN, *IEEE Trans. Dielectr. Electr. Insul.* (2024).
- [24] Z. Wang, J. Zhou, J. Wang, W. Du, J. Wang, X. Han, G. He, A novel fault diagnosis method of gearbox based on maximum kurtosis spectral entropy deconvolution, *IEEE Access* 7 (2019) 29520–29532.
- [25] H.-L. Dang, J. Kim, S. Kwak, S. Choi, Series DC arc fault detection using machine learning algorithms, *IEEE Access* 9 (2021) 133346–133364.
- [26] W. Miao, Q. Xu, K. Lam, P.W. Pong, H.V. Poor, DC arc-fault detection based on empirical mode decomposition of arc signatures and support vector machine, *IEEE Sens. J.* 21 (5) (2020) 7024–7033.
- [27] G. Zou, G. Fu, B. Han, W. Wang, C. Liu, Series arc fault detection based on dual filtering feature selection and improved hierarchical clustering sensitive component selection, *IEEE Sens. J.* 23 (6) (2023) 6050–6060.
- [28] T. Zgonena, L. Ji, D. Dini, Photovoltaic DC arc-fault circuit protection and UL subject 1699b, in: *Photovoltaic Module Reliability Workshop*, Golden, CO, 2011.